Journal of the Korean Physical Society, Vol. 56, No. 1, January 2010, pp. 300∼308

Studying the Role of Ambient Conditions in Laser-induced Al-Plasma Expansion

Galila Abdellatif*
hysics Department, Faculty of Science, Cairo University, Giza, Egypt

Hisham Imam and Yosr E E-D Gamal
National Institute of Laser Enhanced Sciences, Cairo University, Egypt

(Received 31 December 2008, in final form 22 May 2009)

The role of ambient conditions on the spatial and temporal evolution of the aluminum plasma spectral emission is studied. Measurements were carried out in vacuum as well as in air at atmospheric pressure to determine the optimum value of both distances from target and of the delay time at which the spectral line emission is most intense. The plasma is generated using a Q-switched Nd:YAG laser at a wavelength of 532 nm and a pulse duration of 8 ns. The analysis revealed that the intensities of the spectral atomic line (305.00 nm) and the ionic line (281.61 nm) were strongly enhanced in air. Moreover, the plasma expansion velocity was determined using a time-of-flight (TOF) measurements technique. Within the experimentally investigated distance range, its peak value was found to be descending from 1.2×10^5 cm/sec and 5.1×10^4cm/sec in air while in vacuum, it was ascending from 5.0×10^5cm/sec 2.5×10^6cm/sec. In addition, these measurements enabled us to determine the temporal and spatial evolutions of the electron temperature and the electron density by using a Boltzmann plot and a Stark broadening profile, respectively. The estimated values of both the electron temperature and the electron density showed an exponential decrease with time, ending with a leveling off behavior.

PACS numbers: 32.30.r, 52.25.b,52.70.m
Keywords: Laser-induced plasma, Plasma parameters, Aluminum plasma, TOF, Plasma expansion, Electron temperature, Electron density
DOI: 10.3938/jkps.56.300

I. INTRODUCTION

Plasmas produced by laser interactions with solid targets are a promising subject for many fundamental and applied studies. This phenomenon has been studied by several authors; see, for example, Refs. 1-3 and references within, where they used a wide variety of analytical techniques. One of these applied studies is laser propulsion, where the plasma produced from an aluminum target is found to have a tremendous potential to be used as explosives and propellants. It has been used as an explosive to augment air blast, raise reaction temperatures, and create incendiary effects [4] .As a propellant, aluminum has been used to increase the thermal energy and to elevate the flame temperature [5]. Moreover, the application of this phenomenon has importance in remote measurements using laser induced breakdown spectroscopy (LIBS) [6] and in monitoring applications [7]. In these applications, the interaction is designed to operate in open air or in a controllable atmosphere because, compared with vacuum systems, it simplifies the experimental arrangement [8] and is often unavoidable. In addition, the sensitivity of the spectral emission analysis of these plasmas can be dramatically affected by the pressure of the surrounding atmosphere.

In this work, we present a comparative study to analyze the spatial and temporal evolution of the spectral emission of an Al-plasma under different ambient conditions. In doing so, the measurements of the spectral emission are carried out both under vacuum and in air at atmospheric pressure. The effect of these ambient conditions on the plasma parameters and on the plasma expansion velocity is determined. The study aimed to correlate the surrounding ambient conditions with both the distance from target surface and the delay time at which the most intense spectral emission was observed.

II. EXPERIMENTS AND DISCUSSION

A schematic diagram of the experimental arrangement used in this work is shown in Fig. (1). The setup includes

*E-mail: galila.mehena@gmail.com

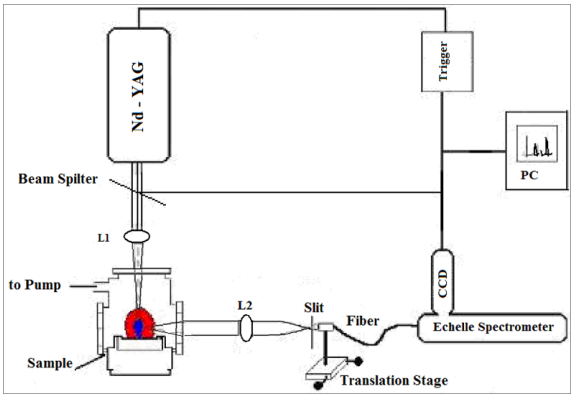

Fig. 1. (color online) Experimental set up.

a Q–switched Nd:YAG laser source (Continuum NY 81-30) operating at 532 nm with a maximum peak energy of 100 mJ in 8ns full width at half maximum (FWHM) at repetition rates up to 30 Hz. The laser beam was focused by using a 20cm convex lens onto the Al-target through a window in the stainlesssteel vacuum chamber. The chamber has several feedthroughs for pumping, pressure gauging, laser entrance, and monitoring. The vacuum chamber is pumped to 10^{-5} mbar by using both rotary and turbo-molecular pumps. The system is provided with a movable target holder that can be rotated or moved back and forth to allow sampling from fresh location on the target surface and to avoid the formation of deep craters, thus improving the reproducibility and accuracy of the spectral emission. The plasma is imaged 1:1 by using a quartz lens with a focal length of 15cm onto the quartz optical fiber entrance. This optical fiber has an aperture of 600 μm in diameter and is mounted on an x-y microtranslation stage. The aperture of the optical fiber is aligned with the central line of the plasma plume to ensure perpendicular collection of the spectral emission with respect to its symmetry axis. The input of the optical fiber is coupled to a slit of 120μm in width to obtain an effective spatial resolution of 150μm. The output of the optical fiber is connected to an Echelle spectrometer (Mechelle 7500) with a focal length of 17cm and an f-number of 5.2. It provides a constant spectral resolution (CSR) of 7500, corresponding to 4 pixels FWHM over a wavelength range of 200 – 900 nm displayable in a single spectrum. A gateable ICCD camera (DiCAM–Pro from PCO computer optics) was coupled to the spectrometer. The overall linear dispersion of the Echelle spectrometer ranges from 0.0078 nm/pixel (at 200 nm) to 0.038 nm/pixel (at 1000 nm).

The instrumental line shape function of the optical system was measured using the emission lines of a mercury lamp and He–Ne laser source to investigate the contours and the widths of the spectral lines. To optimize the signal–to–noise ratio and spectral reproducibility, the acquisition of the spectra was achieved by averaging 50 signals accumulated spectra. The plasma spectral emission was recorded at several distances from the target surface (ranging from 0.25 to 2.0 mm) while varying the delay time from 0 to 4000 ns. These measurements allowed the possibility of determining the position and the delay time of the most intense spectral line. The analysis of the obtained spectral emission was carried out using a commercial 2D and 3D software (GRAMS/32).

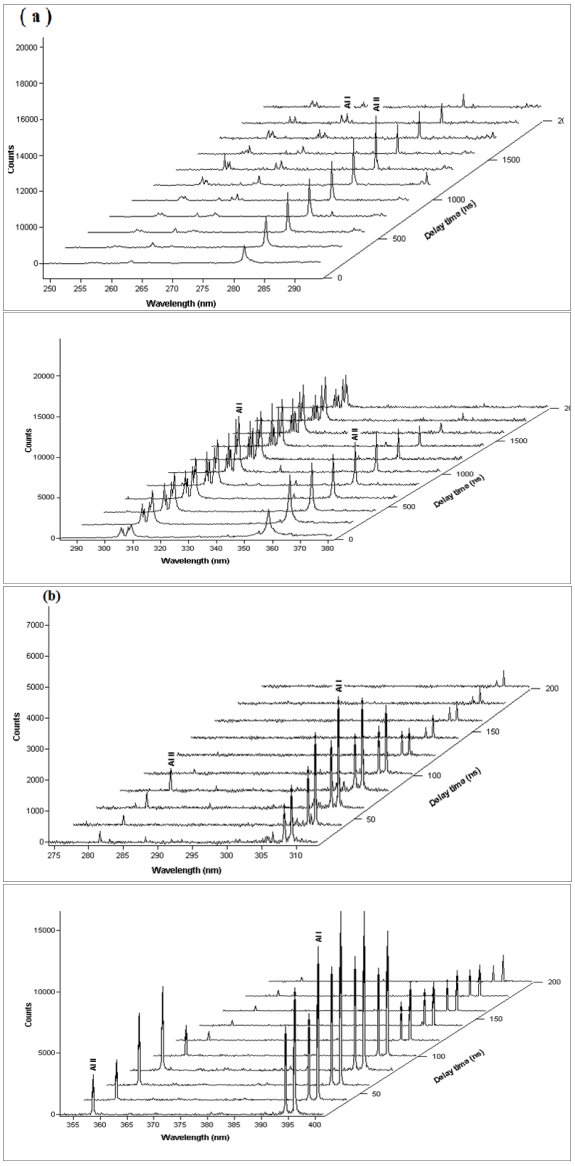

Fig. 2. Temporal evolution of the emission spectrum at 1 mm distance from the target (a) in air and (b) in vacuum.

1. Temporal and Spatial Evolution of an Al Plasma

To study the influence of the ambient conditions on the temporal and spatial evolution of the emission spectra, measurements were carried out to observe the spectra of

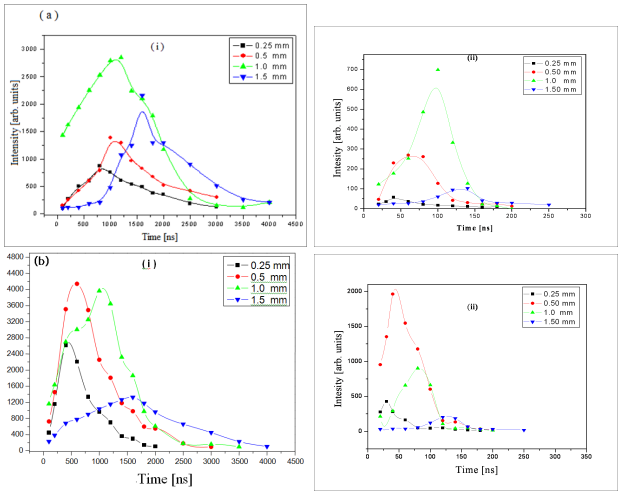

Fig. 3. (color online) (a) Temporal evolution of the emission intensity from the Al I transition at $\lambda = 305.00$ nm in (i) air and in (ii) vacuum at different distances from the target surface. (b) Temporal evolution of the emission intensity from Al II transition at $\lambda = 281.61$ nm in (i) air and in (ii) vacuum at different distances from the target surface.

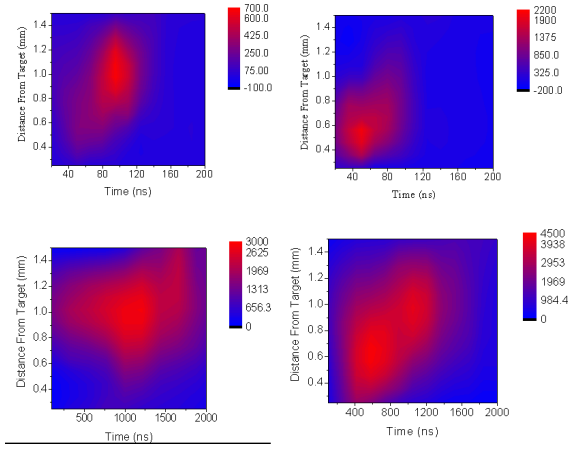

Fig. 4. (color online) Spatial and temporal evolution of the emission intensity from the Al II transition at $\lambda = 281.61$ nm (right) and the Al I transition at $\lambda = 305.00$ nm (left) in vacuum (top) and at atmospheric pressure (bottom).

the Al-plasma plume at different distances from the target surface and at various gate delays of width 50 ns in both vacuum and atmospheric air. The spatial resolution of the spectral emission was obtained by varying the position of the collecting system with respect to the target surface along the central axis of the plasma plume. The analysis was performed to cover a spectral wavelength ranging from 250 nm to 480 nm; this corresponded to the most intense regions of the aluminum plasma emission and included two selected non–resonance spectral lines: namely, Al I at 305.00 nm [3s3p^2-3s3p(^{3}P^0)4s] and Al II at 281.61 nm [3s3p-3s(^{2}S)4s]. The transitions of these two lines have high lower energy levels and small transition probabilities, which strongly lowers the possibility of their self-absorption in the colder parts of the plasma. As an example, Fig. (2) presents the spectral emission of the plasma plume recorded at a distance of 1 mm from the target surface in (i) air and (ii) vacuum.

To gain a deeper insight into the effect of ambient gas conditions on the temporal and spatial evolution of the spectral emission, the relation between the measured line intensity and the delay time was studied and plotted for the abovementioned (a) atomic and (b) ionic lines. These are shown in Fig. (3) in (i) air and (ii) vacuum at distances of 0.25 mm, 0.5 mm, 1 mm, and 1.5 mm. Despite the losses that might occurs in the atmospheric air due to Rayleigh scattering at the selected short wavelengths of the atomic and ionic transitions, in Fig. (3), it is observed that the line intensities recorded in vacuum are much less than those recorded in air. This may be due to a decrease in the electron density during plasma expansion in vacuum. This, in turn, reduces the probability of the ejected species, hence decreasing the spectral line intensity at distances of a few mm away from the target surface. Moreover, Fig. 3(a) shows that the measured emission intensity has the same general behavior in the two environments, where it exhibits a peak followed by a decaying tail. The maximum spectral line intensity is reached after a characteristic time, depending on the examined distance, which corresponds to the most populated section of the plasma plume. This is demonstrated from the measurements in which at a fixed distance, the maximum intensity of the spectral line is reached when the core of the expanding plasma passes in front of the optical collection system. The position of the peak intensity varies according to the nature of the spectral line emission and the surrounding conditions. Based on these measurements, the intense spectral emission of the Al I at 305.00 nm is recorded in both vacuum and air at a distance of 1 mm and at delay times of 100 ns and 1200 ns respectively. For the ionic line emission Fig . 3(b) a similar behavior is shown, where in vacuum the most intense line is recorded at a distance of 0.5 mm corresponding to a delay time of 40ns while in air, two intense lines are observed at distances of 0.5 and 1.00 mm, which correspond to delay times of 600 and 1200 ns, respectively.

It has to be noticed that the lifetime of the excited state of the studied transition is, in all cases, of the order of few ns while the observed increase in emission occurs in times of the order of hundreds of ns. Therefore, one expects that this increase of emission should correspond to species that have been excited during plasma expansion through two main processes: particle collisional excitation and electron–impact excitation/recombination [9, 10]. Knowing that the cross section of the former process is about two orders of magnitude smaller than that of the latter [10 - 12], electron–impact processes are most likely responsible for exciting the plasma species as the plume expands.

To confirm this result, a 2D graph for these intensi-

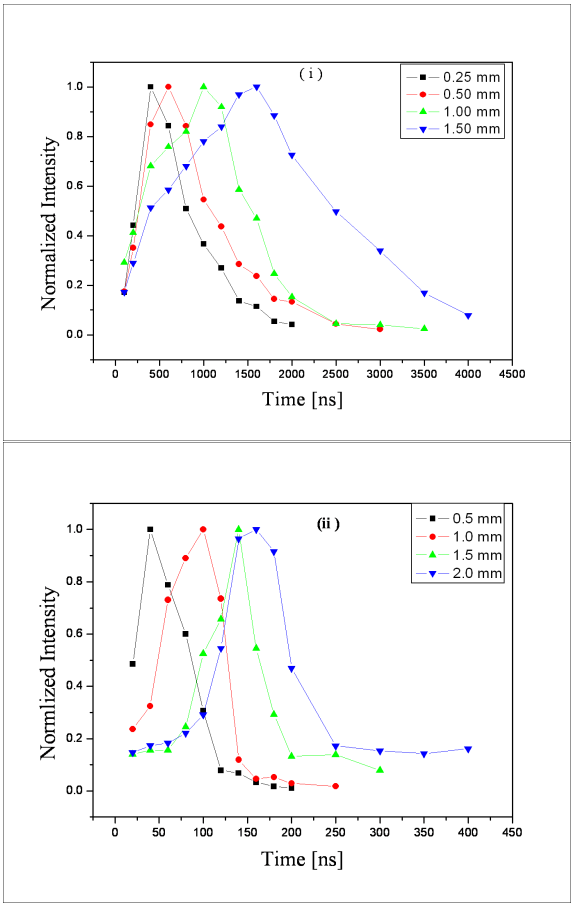

Fig. 5. (color online) TOF profiles of Al II emission intensities at different distances from the target (i) at atmospheric pressure and (ii) in vacuum.

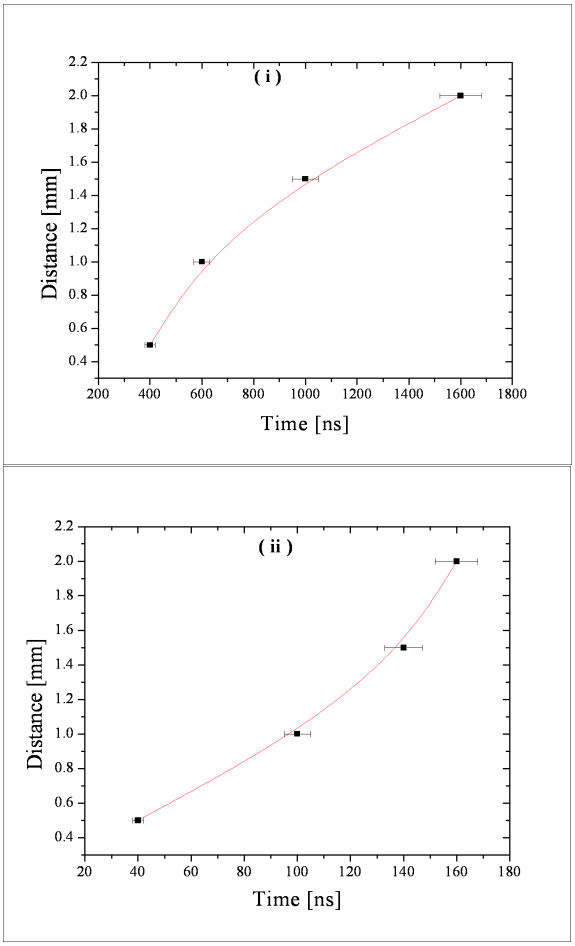

Fig. 6. (color online) Position of the TOF peak at different times: (i) at atmospheric pressure and (ii) in vacuum.

ties is presented in Fig. (4), where the spatial and temporal distributions of the line intensities are shown for wavelengths of 305.00 nm (left) and 281.61 nm (right) in vacuum (top) and in air (bottom). From this figure, it is observed that the line intensities in vacuum are confined to a narrow region closer to the target than they are in air. This region corresponds to the highest temperatures at which the ionization process is enhanced during the plasma expansion. A similar distribution for atomic and ionic line intensities in the plasma was obtained by Sdorra and Niemax [13]. In atmospheric air, however, a more uniform distribution of the light intensity is observed due to reduced energy loss caused by the surrounding air [14].

2. Time - of - flight Measurements

To study the influence of ambient conditions on the mean velocity of the plasma expansion, a time-of-flight (TOF) profile was taken at different distances of the plume in both atmospheric air and vacuum. These profiles were based on optical emission spectroscopy (OES), which offers a simple way to deduce the mean velocity of the plasma expansion in the bright region of the plume over the experimentally examined range (0.25 - 2 mm). The analysis considered the two abovementioned lines: namely, Al I at 305 nm and Al II at 281.6 nm. The time of flight of the atomic emission line is ignored because it is found to present an additional delay due to the three-body recombination, as explained in Ref. 15. Therefore, for the determination of the expansion mean velocity, we considered only the TOF of the ionic line intensities. Accordingly, in Fig. (5), the TOF profile of Al II line is recorded at different distances from the target surface in (i) air and (ii) vacuum. By measuring the shift of the peaks for each distance, Fig. (5) enabled us to obtain a distance - time plot, which is shown in Fig. (6) for (i) air and (ii) vacuum. From this figure, the mean velocity of the plasma expansion was determined and is reported in Fig. (7) and Table 1. These values are found to be in good agreement with the values given in the literature [16–19] . From this figure it is evident that changing the background pressure from vacuum (10^{-5} Torr) to atmo-

Table 1. Peak velocity (cm/s) at different distances from the target at atmospheric pressure and in vacuum.

Distance (mm)	**Peak velocity (cm/s)**	
	Ambient pressure	Vacuum
0.25	1.2 x 10^5	5.0 x 10^5
0.5	1.2 x 10^5	8.3 x 10^5
1	1.0 x 10^5	1.0 x 10^6
1.5	8.1 x 10^4	1.9 x 10^6
2	5.1 x 10^4	2.5 x 10^6

spheric pressure, causes the expansion dynamic to take place in a different manner. Under vacuum conditions, for the experimentally investigated distance range, the mean velocity of the plasma expansion increases with distance. This increase could be attributed to the acceleration of the ablated particles initiated with velocity v_0=0 during the early stages of the laser pulse where the laser energy is less than the ablation threshold. These particles then gain a maximum velocity, v_{max}, at a distance that is probably reached not far from the maximum distance considered here (2 mm) [14, 20]. On the other hand, as is mentioned before in the temporal and spatial resolution of the line intensity, the intensity of the emitted line is reduced as one goes away from the target (i.e. at longer distances). Since the line intensity reflects the density of the emitting species, at longer distances, the plasma density, and hence its collisions, is expected to be reduced. Consequently, the plasma species can keep their energies and move faster in the plume. This can also clarify the case of vacuum where the mean velocity of the plasma increases as the distance increases. At atmospheric pressure, on the contrary, the plasma velocity decreases as the distance increases. This denotes the deceleration of the plasma due to collisions of the ambient gas species with the front head of the plasma, which takes place at very short distances from the target surface.

Generally, over the distance range considered in this analysis, the effect of the radial component of the velocity (divergence of the flow) is ignored. Since at shorter distances, the laser spot on the target surface is assumed to be large enough to minimize lateral expansion, accordingly, the velocity of the plasma is essentially perpendicular to the surface, so the plasma dynamics can be considered one-dimensional [21] .

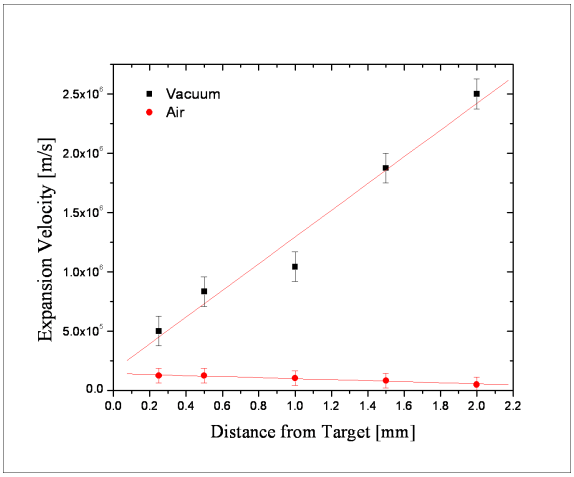

Fig. 7. (color online) Expansion velocity of the plume as a function of the distance from the target: in vacuum and at atmospheric pressure.

3. Plasma Temperature

Measurements were carried out to determine the intensity of the spectral emission lines of the Al plasma at different delay time intervals for each value of the selected distance from the target. Using the well-known Boltzmann plot method and assuming local thermal equilibrium (LTE), the plasma temperature was determined from the relative line intensities of the emission lines according to the relation [22]

$$I_{mn} = F\frac{g_m A_{mn}}{\lambda_{mn} U_z(T_z)} N_z \exp[-\frac{E_m}{kT_z}]. \quad (1)$$

Taking the logarithm of Eq. (1) , we obtain

$$\ln\left[\frac{I_{mn}\lambda_{mn}}{g_m A_{mn}} = m_z + q_z\right]. \quad (2)$$

Here, $q_z = \ln\left[\frac{N_z}{U_z(T_z)}F\right]$ $\qquad m_z = -\frac{E_m}{kT_z}$

where I_{mn} is the intensity of the light emitted during any transition from m→ n (m>n), g_m is the statistical weight of the upper level, k is the Boltzmann constant, λ_{mn} is the wavelength of the emitted photons during the transition from the upper excited energy level E_m to the lower energy level E_n, U_z is the partition function of the species z calculated at T_z, N_z is the concentration of species z in the ground state, and F is an experimental parameter that takes into account the optical efficiency of the collection system, as well as the plasma density and volume.

Table 2. Selected spectral lines of Al II and corresponding spectroscopic data.

Species	λ (nm)	Transition	A (s^{-1}) x10^{-8}	E_i (cm^{-1})	E_k (cm^{-1})	g_i	g_k
Al II	263	3p21D2-3s4f1F^{o}3	0.06	85481	123470		
	281.6	3s3p-3s(^{2}S)4s	3.83	59850	95348	3	1
	358.6	4f^{1}F^0(2,3,4)-3d^{3}D(1,2,3)	2.45	95549	123423	21	15
	466.4	3s3p-3s(^{2}S)4p	0.53	85479	106918	5	3
	365.1	3s4p-3s(^{2}S)5d	0.21	105438	132820	3	5
	559.3	3s4p-3s(^{2}S)5d	1.1	106918	133914	3	5
	623.1	3s4p-3s(^{2}S)4d	0.84	105438	121481	3	5
	624.3	3s4p-3s(^{2}S)4d	1.1	105468	121480	5	7

Table 3. Temporal variation of the electron temperature determined from the Al II at a distance of 1 mm from the target surface in air (left) and in vacuum (right).

Delay (ns)	T_{AlII}(K)	T_{AlII}(eV)	*Delay(ns)*	T_{AlII}*(K)*	T_{AlII}(eV)
600	10950	0.94	80	16500	1.42
800	10800	0.93	100	13700	1.18
1000	10900	0.94	120	13100	1.13
1200	9900	0.85	140	12650	1.09
1400	8900	0.77	160	12300	1.06

Plotting the logarithm of the measured emission intensity for the ionic lines of the Al transitions as a function of the corresponding energy of the upper level, it is possible to obtain a Boltzmann plot for these lines as a function of both distance and time. Table 2 illustrates the selected spectral lines of Al II and their corresponding spectroscopic data [23] .

Figure (8) shows an example of a Boltzmann plot for a selected distance of 1.0 mm from the target surface in vacuum and in air. Using a least-squares fitting technique, the plasma temperature is obtained from the slope of the line fitting the experimental data. This is performed at different time intervals for the examined selected distances. The time evolution of the excitation temperature at different distances from the target and under different environmental conditions is plotted for the Al II lines in Fig. 9 for vacuum (left) and in air (right). This figure show that the overall behaviors of the temporal and spatial variation of the obtained electron temperature are almost the same, where at short distance, the temperature drops fast during the early stages of the delay time, which is followed by a gradual decrease as the time increases. For example at 0.5 mm, values are found to vary from 14900 K (1.28 eV) to 8780 K (0.75 eV) in air and from 24080 K (2.07 eV) to 11480 K (0.99 eV) in vacuum. At longer distances, however, the electron temperature shows a considerably slower variation over the whole delay time range. At 2 mm, values are found to vary from 10000 K (0.86 eV) to 7040 K (0.61 eV) in air and from 15030 K (1.29) to 11140 K (0.96 eV) in vacuum. The high electron temperature shown at distances closer to the target surface is probably due to the fact that immediately after the impact of the laser pulse, electrons absorb enough energy from the laser beam. This in turn leads to an increase in their temperatures. As the plasma expands along the radial distance, electrons may lose their energies in collisional processes with the plasma species, leading to a reduction in their temperatures. Figure (9) clarifies the effect of ambient conditions on the values of the plasma temperature, where in vacuum, its values are found to exceed those obtained in atmospheric air.

4. Electron Density

The electron density is determined by applying the Stark broadening effect for the Al II line at 281.61 nm [4s^{1}S(0) - 3p^{1}P^0(1)]. For an optically thin plasma where self absorption is neglecting for this line, the FWHM of the line ($\Delta\lambda_{1/2}$) is related to the electron density by the expression [22]

$$\Delta\lambda_{1/2} = 2w(\frac{N_e}{10^{16}}) + 3.5A(\frac{N_e}{10^{16}}^{1/4}(1-1.2N_D^{-1/3}w(\frac{N_e}{10^{16}}) \quad (3)$$

where $\Delta\lambda_{1/2}$ is the line width (FWHM), w is the Stark broadening parameter, A is the ion broadening parameter, and N_D is the number of particles in the Debye sphere. In this equation, the first term represents

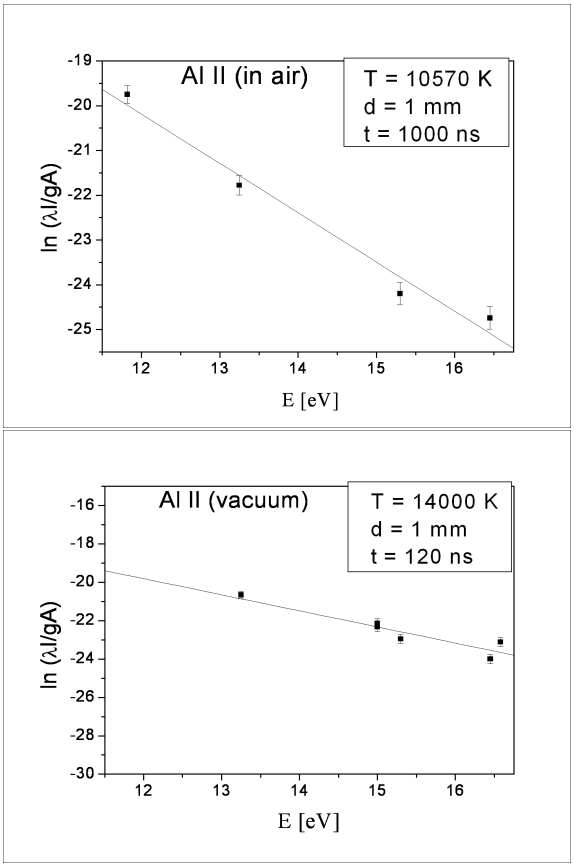

Fig. 8. An example of Boltzmann plots for Al II in air and in vacuum at 1 mm distances from the target.

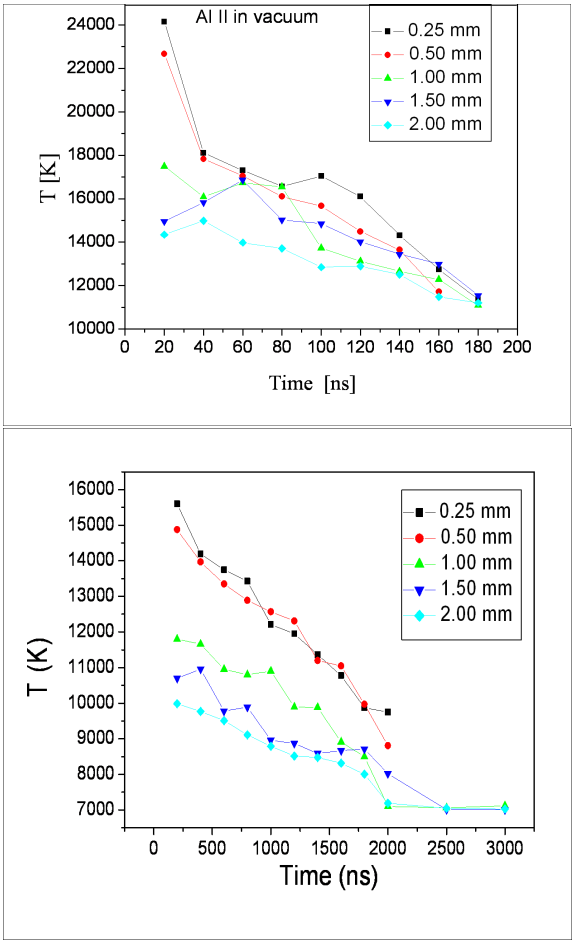

Fig. 9. (color online) Temporal behavior of the plasma temperature obtained via the Boltzmann plot method for Al II under vacuum (left) and in air (right).

the contribution of electron broadening while the second term describes the quasi-static ion broadening contribution. This term is omitted because of it small value in comparison with the first term [24] . Accordingly, Eq. (3) is reduced to

$$\Delta\lambda_{1/2} = 2w(\frac{N_e}{10^{16}}) \quad (4)$$

The observed line shape is corrected by simply subtracting the contribution of the instrumental line broadening through the relation

$$\Delta\lambda_{true} = \Delta\lambda_{observed} - \Delta\lambda_{instrument} \quad (5)$$

The local thermodynamic equilibrium conditions are examined for the selected spectral lines by using the following criterion [24] :

$$N_e(cm^{-3}) \geq 1.6x10^{12}[T_e(K)]^{1/2}[\Delta E(eV)]^3 cm^{-3},$$

where ΔE is the energy difference between the states, which are expected to be in LTE. For all the observed lines, the largest energy difference is approximately 3.65 eV, and the highest electron temperature is found to be about 2 eV. By substituting these values in the above equation, a value is obtained for the electron density of approximately 10^{17} cm^{-3}, which exceeds that value required to maintain the plasma at a LTE condition, 2.3 $\times 10^{16}$ cm^{-3} [25] .

Using Eq. (4) , the temporal evolution of the electron density is obtained at different distances from the target surface for the Al II spectral line (281.61 nm), and the results are presented in Fig. (10). This figure shows that the value of the electron density at atmospheric pressure is higher than that in vacuum; as explained before, this could be due to the electron–impact and confinement processes. During the early stages of plasma evolution, the electron density reaches a value up to 2.5 $\times$ 10^{18} cm^{-3} in vacuum and 6 $\times$ 10^{18} cm^{-3} in atmospheric air at 0.25 mm from the target surface. However, these values drop after a few hundreds of nanoseconds. At a distance of 0.5 mm away from the target surface, the electron density peaks at 1.8 $\times$ 10^{18} cm^{-3} and 4.16 $\times$ 10^{18} cm^{-3} in vacuum and air, respectively. In general, the highest value of the electron density is observed close to the

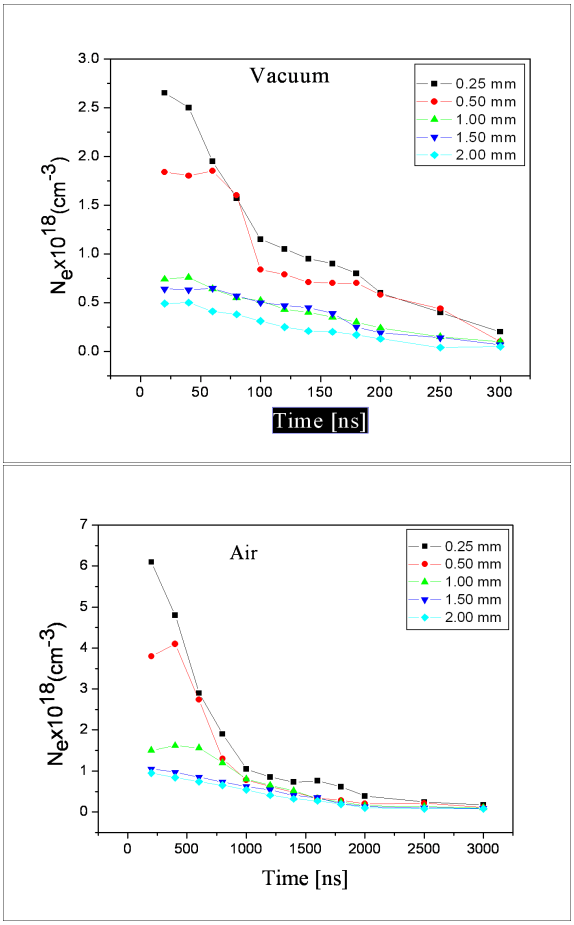

Fig. 10. (color online) Electron density temporal evolution (N_e) at different distances from the target: (a) at atmospheric pressure and (b) in vacuum.

target for the two different ambient conditions; then, it decreases at both longer times and distances from the target. The fast decay rate of the electron density can be attributed to the plasma expansion while the slowing and leveling off (saturation behavior) at longer times are probably due to recombination [26–28]. From this figure it is clear that the temporal electron density shows similar behaviors for examined distances that exceed 0.5 mm away from the target surface, where the electron density suffer a slow decrease as the distance increases.

III. CONCLUSION

The importance of the present experiment is to investigate the influence of the ambient conditions on the spatial and temporal evolution of the spectral emission from a laser - induced Al plasma. This enabled us to determine the position and the time at which the plasma emission was most intense. Consequently, it is possible to use such a plasma as an intense light source. The measurements of the emission were carried out in air at atmospheric pressure and in vacuum. The results of this experiment showed an enhancement of the intensity of the spectral line in the presence of ambient gas. Moreover, it revealed that for the atomic line (Al I - 305.00 nm), the most intense line emission was observed at the same distance for the two ambient conditions, but at an earlier time in the case of vacuum. This indicates that the surrounding air acts to delay the appearance of spectral emission for time intervals exceeding more than 10 times those measured in vacuum. For the ionic line (Al II - 281.61 nm), the intense emission appeared at a closer distance to the target (0.5 mm) in vacuum while in air, it was observed for the two distances (0.5 and 1.0 mm) at longer delay times.

Using the optical TOF technique, the expansion velocity of the plasma induced by laser radiation was measured for both air and vacuum. The measurements demonstrated that very different regions of plasma expansion occur under the different ambient conditions considered here. Moreover, the analysis of the plasma optical emission facilitated the measurement of the temporal and spatial profiles of the plasma electron temperature and density during plasma expansion, both in vacuum and in atmospheric air.

ACKNOWLEDGMENTS

This work was supported by a grant from the Korean Ministry of Education, Science and Technology (The Regional Core Research Program/Center for Healthcare Technology Development).

REFERENCES

[1] E. H. Piepmeier, *Analytical Applications of Lasers* (Wiley, New York, 1979).
[2] L. J. Radziemsky and D. A. Cremers, *Laser-Induced Plasmas and Applications* (Marcel Dekker, New York, 1989).
[3] W. B. Lee, J. Wu, Y.-I. Lee and J. Sneddon, Appl. Spectrosc. Rev. **39**, 27 (2004).
[4] S. Yuasa, Y. Zhu and S. Sogo, Combust. Flame **108**, 387 (1997).
[5] D. C. Mueller and S. R. Turns, J. Propul. Power **12**, 591
[6] E. Tognoni, V. Palleschi, M. Corsi. and G. Cristoforetti, Spectrochim. Acta, part B **57**, 1115 (2002).
[7] D. Bäuerle, *Laser Processing and Chemistry* (Springer-Verlag, New York, 2000).
[8] Thuvan N. Piehler, Frank C. De Lucia Jr., Chase A. Munson, Barrie E. Homan, Andrzej W. Miziolek, and Kevin L. McNesby, Appl. Optics **18**, 44, 3654 (2005).
[9] C. Timmer, S. K. Srivastava, T. E. Hall and A. Fucaloro, J. Appl. Phys. **70**, 1888 (1991).
[10] H. F. Sakeek, T. Morrow, W. G. Graham and D. G. Walmsley, J. Appl. Phys. **75**, 1140 (1994).
[11] H. S. Kwok, Thin Solid Films **218**, 277 (1992).

[12] H. P. Gu, Q. H. Lou, N. H. Cheung, S. C. Chen, Z. Y. Wang and P. K. Liu, Appl. Phys. B **58**, 143
[13] W. Sdorra and K. Niemax, Mikrochim. Acta **107**, 319 (1992).
[14] J. Hermann, C. Boulmer Leborgne and D. Hong, J. Appl. Phys.**83**, 691 (1998).
[15] H. Imam, G. Abdellatif, V. Palleschi, M. A. Harith and Yosr E-El. Gamal, MTPR-06 AIP
[16] J. C. S. Kools, T. S. Baller, S. T. De Zwart and J. Dieleman, J. Appl. Phys. **71**,4547 (1992).
[17] J. Hermann, A. L. Thomann, C. Boulmer-Leborgne, B. Dubreuil, M. L. De Giorgi, A. Perrone, A. Luches and I. N. Mihailescu, J. Appl. Phys. **77**, 2928 (1995).
[18] X. T. Wang, B. Y. Man, G. T. Wang, Z. Zhao, B. Z. Xu, Y. Y. Xia, L. M. Mei and X.Y. Hu, J. Appl. Phys. **80**, 1783 (1996).
[19] A. De Giacomo, V. A. Shakhatov, G. S. Senesi and S. Orlando, Spectrochim. Acta B **56**, 1459 (2001).
[20] M. Capitelli, A. Casavola, G. Colonna and A. De Giacomo, Spectrochim. Acta B **59**, 271 (2004).
[21] J. Hermann, C. Boulmer-Leborgne and D. Hong, J. Appl. Phys. **83**, 691 (1998).
[22] H. R. Griem, *Plasma Spectroscopy* (Mc Graw-Hill, New York, 1964).
[23] J. Reader, C. H. Corliss, W. L. Wiese and A. G. Martin Wavelengths and Transition Probabilities for Atoms and Atomic Ions, NSRDS-NBS 68, National Bureau of Standards, Washington (1980) and NIST Atomic Spectra Database. Available from (www.physics.gov).
[24] G. Bekfi, *Principles of laser plasma* (Wiley, New York, 1976).
[25] G. Abdellatif and H. Imam, Spectrochim. Acta B **57**, 1155 (2002).
[26] C. Aragon, J. Bengoechea and J. A. Aguilera, Spectrochim. Acta B **56**, 619 (2001).
[27] N. Tsuda and J. Yamada, Eur. Chem. Abstr. **22c**, 922 (1998).
[28] Abd El-Hameed, G. H. Abou-Koura, and Y. E. Gamal, Nucl. Instrum. Meth. B **205,** 1 (2003).